Journal of Atmospheric and Solar-Terrestrial Physics 183 (2019) 11–18

Contents lists available at ScienceDirect

Journal of Atmospheric and Solar-Terrestrial Physics

journal homepage: www.elsevier.com/locate/jastp

Numerical simulation of the mean meridional circulation in the middle atmosphere at different phases of stratospheric warmings and mountain wave scenarios

Andrey V. Koval[a,*], Nikolai M. Gavrilov[a], Alexander I. Pogoreltsev[a,b], Ekaterina A. Drobashevskaya[b]

[a] Atmospheric Physics Department, Saint-Petersburg State University, Saint-Petersburg, 198504, Russia
[b] Department of Meteorological Forecasts, Russian State Hydrometeorological University, Saint-Petersburg, Russia

ARTICLE INFO

Keywords:
Meridional circulation
Sudden stratospheric warming
Orographic gravity waves
Numerical modeling

ABSTRACT

In this study, numerical simulations have been performed to estimate the transformation of the mean meridional circulation in altitude range 0–100 km at different phases of simulated stratospheric warming (SW) events in January–February including and excluding impact of mesoscale orographic gravity waves (OGWs). To obtain an ensemble of 12 pairs of model runs with and without a parameterization of OGW effects, the numerical middle and upper atmosphere model (MUAM) has been used. Obtained results demonstrate weakening of the zonal mean meridional circulation at altitudes up to 100 km during and after simulated SWs compared to the time interval before SWs. At altitudes below 50 km, southward mean meridional winds decrease (up to 15%) before and after simulated SWs. OGW effects may increase the mean northward wind at altitudes above 60 km up to 10–15%. The most significant changes of the meridional circulation in the middle atmosphere are detected at the middle and high latitudes of the Northern Hemisphere: the southward meridional circulation increases at altitudes above 40 km and decreases below 40 km. Thus, the global-scale mean meridional circulation in the middle atmosphere may significantly depend on different phases of SW events during the northern winter season. It is also quite sensitive to the dynamical and thermal OGW impacts.

1. Introduction

Dynamical interactions between tropospheric and stratospheric layers have recently received increasing attention. These interactions intensify during sudden stratospheric warming (SSW) events, which consist of substantial temperature increases (up to 30–40 K) at high northern latitudes at altitudes 30–50 km and simultaneous decreases (or reversals) of the zonal-mean eastward velocity in the stratospheric Polar Vortex (e.g., McInturff, 1978; McIntyre, 1982). SSW development depends on breaking of planetary waves (PWs), which propagate from the lower atmosphere (e.g, Quiroz, 1975; Labitzke, 1977; Schoeberl, 1978). During recent years, increasing interest exists in the investigation of influence of SSWs on the formation of weather anomalies and climate changes in the troposphere (e.g. Baldwin et al., 2001, 2007; Masakazu, 2003; Sun and Robinson, 2009; Nath et al., 2016). SSW events can also substantially affect the dynamics and energetics of the upper atmosphere (Siskind et al., 2010; Kurihara et al., 2010; Fuller-Rowell et al., 2010; Funke et al., 2010; Liu et al., 2011; Yuan et al., 2012), so they can influence the space weather. Many SSW characteristics were analyzed from observations (e.g., Labitzke and Kunze, 2009; Kuttippurath and Nikulin, 2012). Changes in meridional circulation during different phases of SSW event were recently studied by Tao et al. (2017), de la Camara et al. (2018). However, many issues remain unclear, especially relating to SSW formation mechanisms and SSW impacts on gravity and planetary wave interactions (Albers and Birner, 2014).

Energy and momentum transport by internal waves is important factor influencing dynamical coupling of the middle and lower atmosphere (Andrews et al., 1987; Buhler, 2009). Essential sources of mesoscale waves are inhomogeneities of the Earth's surface (Gossard and Hooke, 1975). Generation of mountain, or orographic gravity waves (OGWs) by the surface relief and transport of their energy and momentum upwards can significantly alter the general circulation and PW parameters, and, hence, produce changes in the SSW development. PWs and gravity waves interactions in the atmosphere were studied by McLandress and McFarlane (1993), Cohen et al. (2013, 2014) and

* Corresponding author.
E-mail address: a.v.koval@spbu.ru (A.V. Koval).

https://doi.org/10.1016/j.jastp.2018.12.012
Received 28 July 2018; Received in revised form 26 December 2018; Accepted 28 December 2018
Available online 29 December 2018
1364-6826/

Sigmond and Shepherd. (2014).

Simplified schemes exist for parameterizing dynamical and thermal OGW impacts (e.g., Kim and Arakawa, 1995; Lott and Miller, 1997; Scinocca and McFarlane, 2000; Vosper and Brown, 2007; Catry et al., 2008; Geller et al., 2011). Most parameterizations do not calculate vertical profiles of heat influxes and wave acceleration caused by stationary OGWs, which requires taking into account the Earth's rotation. Gavrilov et al. (2013a, 2013b) developed and implemented a parameterization of dynamical and thermal effects of stationary OGWs into a mechanistic numerical model simulating general circulation at altitudes from the troposphere up to the thermosphere. They showed that OGWs could significantly affect the general atmospheric circulation in the middle and upper atmosphere.

Gavrilov et al. (2018) investigated the interaction between OGWs and PWs during stratospheric warming (SW). Koval et al. (2018) researched the features of PW generation and propagation in the middle and upper atmosphere under different phases of quasi-biennial oscillations (QBO) of the low-latitude zonal wind during SSW event. It was shown that amplitudes of stationary PWs in the middle atmosphere of the Northern hemisphere might differ up to 30% at different QBO phases before and during SSWs.

In the present study, we focus on the changes in the mean meridional atmospheric circulation at altitudes 0–100 km during time intervals before, during, and after SWs simulated in the general circulation Middle and Upper Atmosphere Model (MUAM) with and without taking into account the OGW dynamical and thermal impact. Such detailed studies of the influence of SW phases and mountain waves on the mean meridional circulation up to high altitudes is carried out for the first time. For a long time, there was a misconception that mechanistic general circulation models with a relatively low resolution cannot reproduce major SSWs. Pogoreltsev et al. (2014) showed that inclusion of normal atmospheric modes can allow mechanistic models to simulate SSWs. MUAM is one of a mechanistic GCM able to reproduce major stratospheric warmings.

2. The numerical model

In order to investigate the dependence of the atmospheric dynamics during SW events, we used a three-dimensional numerical model of general atmospheric circulation MUAM (Pogoreltsev, 2007; Pogoreltsev et al., 2007). The model architecture is based on the finite-differences Cologne Model of the Middle Atmosphere-Leipzig Institute for Meteorology (COMMA-LIM; Fröhlich et al., 2003). The main equations and physical processes used in the model were described by Gavrilov et al. (2005). The horizontal grid of the model has 36 equidistant steps along the latitudes and 64 grids along the longitudes. As the vertical coordinate, the log-isobaric height with 48 vertical levels at the altitudes from the ground to 135 km is used.

Radiation block of the MUAM is able to calculate solar heating and infrared cooling rates of the most prominent absorbers and emitters in the middle atmosphere, such as NO, O, O_2, O_3, H_2O and CO_2 (Fröhlich et al., 2003). The model involves parameterizations of radiation heating the atmosphere in the ultraviolet and visible spectral bands from 125 to 700 nm and cooling in the 8, 9.6, 14 and 15 mkm infrared bands accounting breakdown of the local thermodynamic equilibrium at high altitudes.

For the proper simulations of the middle and upper atmosphere dynamics, the calculation of dynamical and thermal effects of non-orographic gravity waves (GWs) are required (Andrews et al., 1987). As these GWs have scales smaller than the MUAM grid spacings, parameterization scheme, similar to the Lindzen's one (Lindzen, 1981) is used. Stationary planetary waves in the MUAM are generated by specifying climatological temperature and wind near the lower boundary (Koval et al., 2018). The model can simulate also travelling modes (Pogoreltsev et al., 2014). The sources of westward propagating atmospheric normal modes (NMs) in the troposphere are parameterized by inclusion of additional terms to the equation of heat balance, which involve sets of time series of sinusoidal components with periods corresponding to NMs marked as (1,1), (1,2), (1,3), (2,1) and (2,2) in the classification by Longuet-Higgins (1968). Latitude structures of these terms correspond to the Hough functions of respective NMs calculated with the algorithm by Swarztrauber and Kasahara (1985). The amplitudes of NM heat sources at altitude of 10 km are applied. These heating sources give simulated NM amplitudes comparable with the observed ones in the stratosphere (Pogoreltsev et al., 2009).

The initial condition for numerical simulations is a windless state with the constant temperature profile. For the MUAM adjustment, geopotential heights at the lower boundary are set to be independent on longitude in the first 30 model days. Then, the longitudinal geopotential variations (stationary planetary waves) corresponding to the UK Met Office database (Swinbank and O'Neill, 1994) are specified. Before the model day of 121, the MUAM involves the daily-mean heating rates only. The tests described by Pogoreltsev (2007) showed that described procedures are enough for the model to reach a steady-state regime at the end of this time interval. The prognostic equation for temperature in the MUAM contains an additional term proportional to the difference between calculated and observed climatological temperatures in the stratosphere by the UK Met Office reanalysis database for January. The constant of proportionality is inversely to characteristic time ($\sim$5 days) of relaxation of the calculated temperature to the observed one. After the 121th day, daily variations of heating, parameterization of the normal atmospheric modes and an additional prognostic equation for the geopotential perturbation at the lower boundary are included. This prognostic equation needs to satisfy the lower boundary condition for the waves generated by internal sources (Pogoreltsev et al., 2007, 2009). Starting from 330th model day, seasonal changes in solar heating are triggered and the next 60 days are considered as characteristic for January–February.

The simulated in the MUAM parameters include geopotential, temperature, as well as zonal, meridional and vertical wind components. For the time integration, the scheme proposed by Matsuno (1966) is used. The integration time step is 450 s.

For examining the influence of OGWs on atmospheric dynamics, the parameterization of dynamical and thermal effects of stationary OGWs (Gavrilov and Koval, 2013) was implemented into the MUAM. This parameterization performs calculations of vertical profiles of OGW amplitudes, total vertical wave energy flux and accelerations of horizontal wind produced by stationary OGWs. The mesoscale topography is parameterized using the method of so-called "subgrid orography" that takes into account altitude variations of the Earth surface with horizontal scales smaller than the horizontal grid step of the MUAM (Scinocca and McFarlane, 2000; Lott and Miller, 1997). Earth surface relief in the OGW parameterization is given by the ETOPO2 (2015) database with resolution of 2 angle minutes in latitude and longitude. The stages of initialization of the MUAM are described in details by Pogoreltsev et al. (2007) and Gavrilov et al. (2018).

The development of stratospheric warming depends on the phases of stratospheric vacillations of zonal wind and PW characteristics (e.g., Holton and Mass, 1976). In the MUAM, the changes in phases of stratospheric vacillations can be attained by changing the starting day of the daily variations of solar heating during the initial model adjustment (see Pogoreltsev, 2007). In the 12 pairs of the MUAM runs (with and without OGW parameterization, respectively), the starting day for the diurnal variability of the solar heating was changed between 120th and 142th model days with the step of 2 days.

3. Results of simulations

To achieve statistical significance, a set of 12 pairs of the MUAM runs (including and excluding OGW parameterization) was obtained. This approach allowed us to obtain a set of simulated SW events statistically similar to SW climatology obtained from multi-year reanalysis

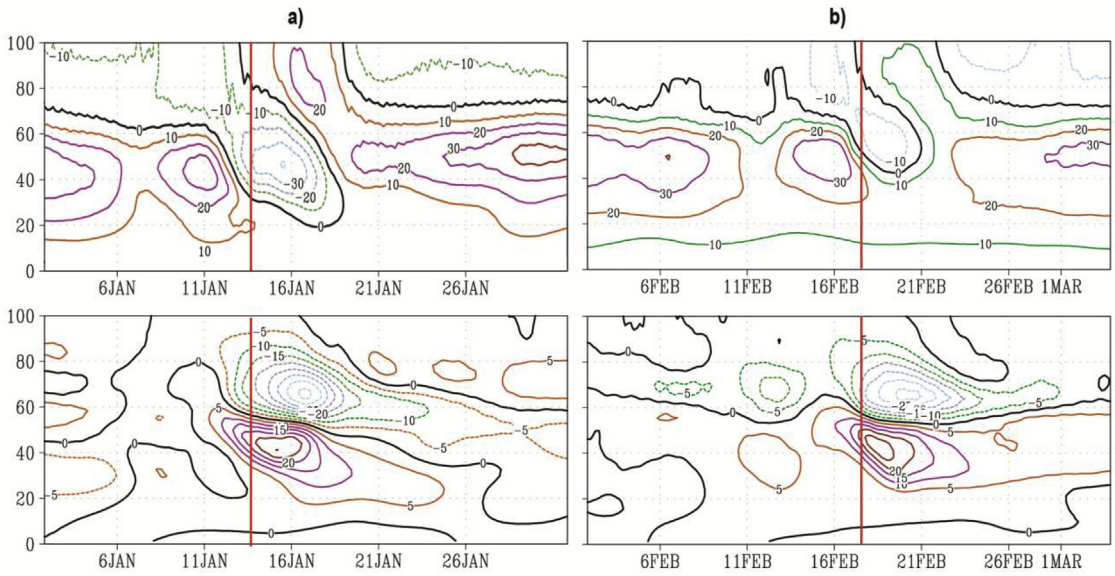

Fig. 1. Examples of simulated evolutions of the zonal-mean zonal wind at 62.5°N (top) and deviation from the monthly-mean temperature at 82.5–87.5°N (bottom) for two different MUAM runs (a and b). Vertical lines show SW starting dates obtained with the method described in section 3.

data and described by Savenkova et al. (2017).

3.1. Determination of SW phases

In each MUAM run, the simulations showed existence of minor or major stratospheric warming events during January–February. The dates of major and minor warming events were chosen by using the definitions by Charlton and Polvani (2007), however the zonal wind decreases and reversals were detected not only at the traditional pressure level of 10 hPa, but at higher altitudes up to 50 km in each MUAM run similar to Gavrilov et al. (2018). Types of stratospheric warming events differ for model runs within the ensembles mentioned above. Examples of stratospheric warmings simulated at different MUAM runs are presented in Fig. 1 where vertical lines show the SW dates obtained as described above.

The top panel of Fig. 1a reveals the reversal of the zonal-mean zonal wind at 62.5°N at altitude of 30 km during SW, while in the top panel of Fig. 1b the wind reversal occurs only at altitudes above 45 km. Fig. 1a corresponds to traditional major SSW usually associated with sharp temperature increases and wind reversal at the 10 hPa pressure level (e.g., Butler et al., 2015). Savenkova et al. (2017) analyzed SW manifestations based on the multi-year statistics of retrospective analyses of meteorological reanalysis data and found frequent reversals of the mean zonal wind at altitudes higher than 40 km.

In our modeling, the starting dates of simulated SW varies between different model runs and depends on the phases of stratospheric vacillations at altitudes 20–60 km at high northern latitudes. Similarly to SW climatology by Savenkova et al. (2017), simulated SWs frequently occur above the 10 hPa pressure level. To differentiate warming events simulated in our model at higher altitudes from traditionally considered SSWs, we call them below as “stratospheric warmings” (SWs) as it was proposed by Gavrilov et al. (2018). Comparisons of Fig. 1a and b allows us to conclude that changes in phase of stratospheric vacillation can produce SW events at different altitudes between 20 and 60 km. We calculated average over the 12-member ensemble of the MUAM runs characteristics of composite SW and compared them with those obtained from the multi-year MERRA reanalysis data base (Rienecker et al., 2011). Both simulated and observed deviations of the mean temperature have maxima at altitude of about 40 km.

We performed modeling to calculate the mean meridional and vertical velocity in the atmosphere at different phases of simulated SW events and made 12 pairs of the MUAM runs with and without OGW parameterization using the same set of the initial data. We chose three consecutive 11-day intervals (one before and two after the starting date of each simulated SW), which are referred thereafter as “before”, “during” and “after” SW, and averaged simulated characteristics respectively for each time interval over 12 MUAM runs, similarly to Gavrilov et al. (2018).

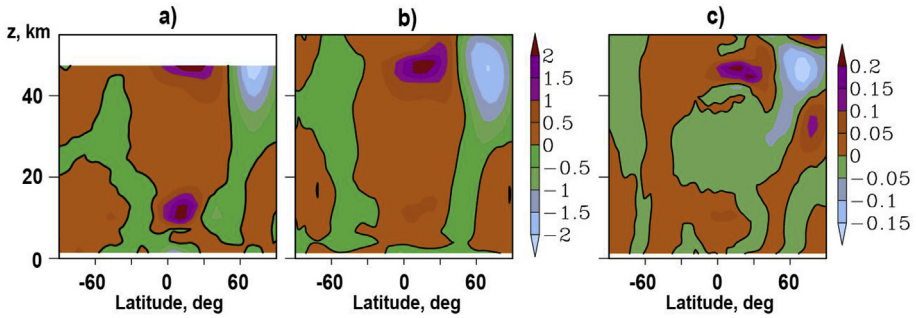

Fig. 2. January zonal-mean meridional wind (in m/s) from the JRA-55 reanalysis database averaged over the years 1995–2013 (a), averaged over 12 MUAM runs without OGW parameterization (b) and average differences in the meridional velocities simulated with and without OGW dynamical and thermal effects (c).

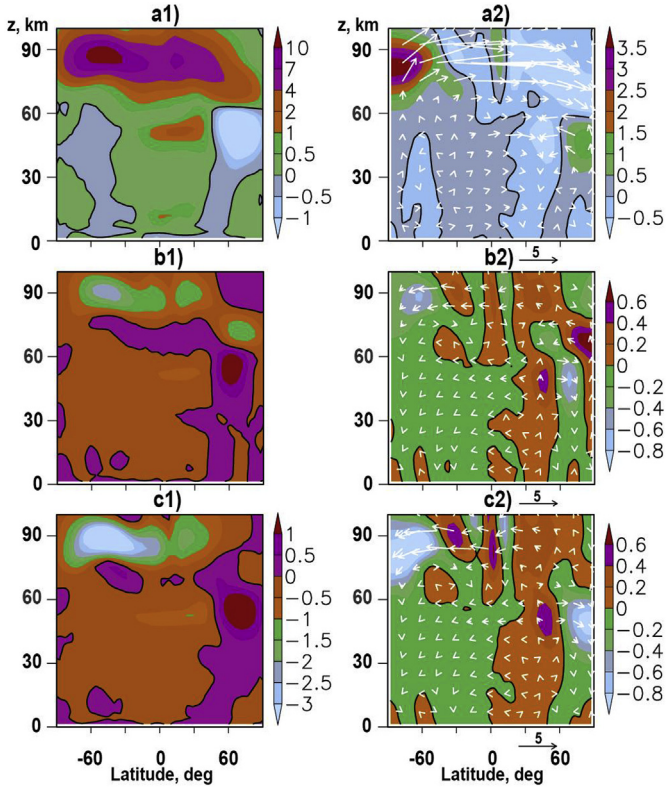

Fig. 3. Zonal-mean meridional velocity in m/s (a1) and vertical velocity in cm/s (a2) simulated with the MUAM and averaged over 12 model runs for 11-day intervals before SW (a1). Arrows show velocity vectors in the meridional plane in m/s (vertical component is multiplied by 100 for the sake of illustration); (b) and (c) show corresponding differences between the time intervals during and before (b), also after and before (c) simulated SWs. Solid contours correspond to zero levels.

3.2. Zonal-mean meridional circulation

Fig. 2a presents the latitude-height distribution of the January zonal-mean meridional velocity obtained from the reanalysis of the meteorological information JRA-55 (Japanese 55-year Reanalysis) database (Kobayashi et al., 2015) and averaged over the years 1995–2013. For comparison, Fig. 2b shows simulated distribution of the same velocity averaged over January and over 12 model runs excluding OGW parameterization from the MUAM. The general similarity between observed and simulated distributions in Fig. 2a and b below 50 km can be seen. Detailed considerations of Fig. 2 at altitudes about 10 and 50 km in the Northern Hemisphere reveal smaller peak magnitudes of northward and southward velocities simulated with the MUAM excluding OGW parameterization (Fig. 2b) compared to the observed ones in Fig. 2a. Changes in meridional velocities which are revealed in Fig. 2c bring the results of simulations closer to the observed or assimilated ones (see Section 3.4). A similarity between observed and simulated meridional velocities was also found from comparisons of the MUAM results with the reanalysis databases UK Met Office model (Swinbank and O'Neill 1994) and MERRA-2 (Gelaro et al., 2017).

Fig. 3a1 shows simulated distribution of the zonal-mean meridional velocity averaged over 11-day intervals before simulated SW and over 12 model runs including OGW parameterization into the MUAM. Below 60 km, this distribution is very similar to those given in Fig. 2a and b. Fig. 3a2 presents the zonal-mean vertical velocity and vectors reflecting zonal-mean circulation in meridional plane averaged over 12 MUAM runs including OGW dynamical and thermal effects. Joint considerations of Fig. 3a demonstrate that the main cell of the mean meridional circulation at altitudes higher than 60 km has upward flow at high and middle latitudes of the Southern Hemisphere, northward wind and downward flow in the Northern Hemisphere. In Fig. 3a2 below 50 km altitude, the Brewer-Dobson convective cells can be seen. These cells have ascending flows at low latitudes and descending flows at middle latitudes, especially noticeable in the Northern Hemisphere (Butchart et al., 2006). A polar vortex, existing at high latitudes of the winter hemisphere, can contribute to additional upward vertical velocities up to 2 cm/s at latitudes of 60–90° N and altitudes 20–60 km. This may intensify respective increases in downward flows at latitudes 50–70° N and form a local sub-cell of circulation in the strato-mesosphere of the Northern Hemisphere noticeable in Fig. 3a. Similar upward flows exist near the South Pole in Fig. 3a2. However, below the altitude of 60 km upward vertical velocity does not exceed 0.5 cm/s there and increases up to 4 cm/s at mesopause altitudes 80–90 km at high latitudes of the Southern Hemisphere.

Upward or downward displacements of atmospheric air parcels lead to their adiabatic cooling or heating, respectively. Therefore, downward flows in the Northern Hemisphere and upward flows in the Southern Hemisphere (see Fig. 3a2) can contribute to the warmer atmosphere near the North Pole and cooler atmosphere near the South Pole above altitude of 60 km in January–February. Similarly, upward vertical velocities at altitudes 20–60 km at high northern latitudes in Fig. 3a2 can contribute to cooling of the stratosphere near the North Pole and to a strengthening of the Polar Vortex in winter.

Fig. 3b1 shows differences in the zonal-mean meridional velocity between the 11-day intervals during and before simulated SWs averaged over 12 MUAM runs. Fig. 3c1 represents similar differences for the time intervals after and before simulated SWs. Fig. 3b2 and 3c2 demonstrate differences in the zonal-mean vertical (shaded) velocities and meridional circulation (arrows) between the 11-day intervals during and before (Fig. 3b2) and after and before (Fig. 3c2) averaged over 12 MUAM runs including OGW parameterization. The hypothesis of nonzero differences in Fig. 3b and c can be verified with the statistical Student's t-test (Rice, 2006). In each MUAM grid point, we have $66 \times 64 \times 12 = 50688$ pairs of values in time and longitude (11 days with 4-h outputs, 64 latitude points, 12 model runs). Paired t-tests showed higher than 95% confidences of nonzero differences of meridional and vertical velocity at all latitude-altitude model grid points where their absolute values in Fig. 3b and c are larger than 0.2 m/s and 0.1 cm/s, respectively.

Comparisons of Fig. 3b2 and 3a2 disclose positive vertical velocity differences during simulated SWs at altitudes 60–80 km and latitudes 60–90° N and generally negative differences at altitudes below 60 km. This corresponds up to 100% weakening of downward flows in Fig. 3b2 above altitude of 60 km and up to 40–50% weakening of upward flows below 60 km existing before SWs at high northern latitudes. Associated changes in adiabatic heating rates can significantly contribute to further heating the stratosphere and cooling the mesosphere during simulated SWs. In time intervals after simulated SWs in Fig. 3c2, the vertical velocity differences remain positive in the Northern Hemisphere at altitudes above 60 km and generally negative at latitudes 60–90° N and altitudes below 60 km. These signs are opposite to the vertical velocity signs in Fig. 3a2 before simulated SWs and correspond to general weakening of the global meridional circulation cell at high altitudes and the local upward flows in the high-latitude northern stratosphere described above.

In the Southern Hemisphere, the main differences in the zonal-mean meridional and vertical velocities in Fig. 3b and c during and after simulated SWs exist at altitudes above 70 km and have signs generally opposite to the respective velocities in Fig. 3a before SWs. Absolute values of the differences are larger after SWs than those during SWs. This means weakening of northward velocity at altitudes 80–100 km in the mid-latitude Southern Hemisphere up to 25–30% during SWs and up to 30–40% after SWs compared to that before warming events. Respective decreases in the upward velocity near the high-latitude mesopause in the Southern Hemisphere can reach 20–30% during SWs and

30–40% after SWs. Such changes may be produced by the weakening of meridional circulation in the Northern Hemisphere discussed above and associated with SW events, which can influence the entire global circulation. From this point of view, the larger velocity differences in the later time intervals after SWs in Fig. 3c may reflect a time delay, which is needed for the Southern Hemisphere circulation to "feel" changes in the Northern Hemisphere. Larger differences in the Southern Hemisphere circulation after SWs also could partly reflect seasonal changes in the global meridional circulation, as far as time intervals after SWs have permanent 3-week time delay compared to respective intervals before SWs.

Arrows in Fig. 3a2 show the average zonal-mean velocity vectors in the meridional plane corresponding to the meridional and vertical velocities shown in Fig. 3a for the 11-day time interval before simulated SW events. Vertical wind component in Fig. 3a2 is multiplied by factor 10^2 for better illustration. The arrows represent discussed above global circulation cell from the Southern to the Northern Hemisphere above altitude of 60 km, the Brewer-Dobson circulation cell below 50 km and upward flows at the high-latitude Northern Hemisphere at altitudes 20–60 km.

Arrows in Fig. 3b2 and 3c2 show differences in the zonal-mean velocity vectors in the meridional plane between respective intervals during and after simulated SW events and 11-day intervals before SWs, which are averaged over 12 MUAM runs. In most cases, arrows in Fig. 3b2 and 3c2 are directed opposite to the respective arrows in Fig. 3a2. This shows that the meridional circulation cells discussed above become generally weaker during and after simulated SWs, than they were before SWs, as it was discussed earlier.

To diminish random fluctuations, we considered zonal-mean meridional and vertical winds averaged over different latitudinal bands, which are discussed in the following section.

3.3. Latitudinal band characteristics

To study integral effects, we averaged the zonal and meridional wind components over 30° latitude bands in both hemispheres. Figs. 4 and 5 represent, respectively, the zonal-mean meridional and vertical velocity components averaged over latitude bands 0–30°, 30–60° and 60–90° (lines marked as 1–3, respectively) of the Northern and Southern Hemispheres for 11-day intervals before, during and after simulated SW. Solid lines in Figs. 4 and 5 show velocity components simulated including OGW parameterization to the MUAM. Above altitude of 60 km in Figs. 4 and 5, a meridional cell dominates with northward meridional velocities and ascending vertical flows in the Southern Hemisphere and descending vertical motions in the Northern Hemisphere. At altitudes 15–60 km, downward vertical flows dominate at latitudinal band of 30–60° N with upward vertical flows at 60–90° in Fig. 5. These vertical flows have largest magnitudes before simulated SWs in Fig. 5a1, become smallest during SWs in Fig. 5b1 and then recover after SW in Fig. 5c1, but are still smaller, then before warming event.

In the Southern Hemisphere in the bottom panels of Figs. 4 and 5, the largest meridional and vertical velocities exist at high latitudes at altitudes above 60 km. Largest and smallest vertical velocities exist before and after SWs in Fig. 5a2 and 5c2, respectively. This may reflect a time delay in the Southern Hemisphere reaction on the changes of the meridional circulation in the Northern Hemisphere during SWs and possible seasonal changes in atmospheric circulation (see section 3.1).

Our simulations show that global-scale meridional circulation in the middle atmosphere may significantly vary during different phases of the simulated SW events in the northern winter.

3.4. OGW influence on the zonal-mean meridional circulation

Described above numerical modeling allows us to estimate the sensitivity of meridional circulation to the OGW dynamical and thermal impact at different SW phases. We made 12 pairs of the MUAM runs with and without OGW parameterization using the same set of the initial data. The differences between these pairs of simulations demonstrate OGW impact on the meridional circulation. Positive or negative differences correspond, respectively, to increases or decreases in velocity components due to OGW thermal and dynamical impacts.

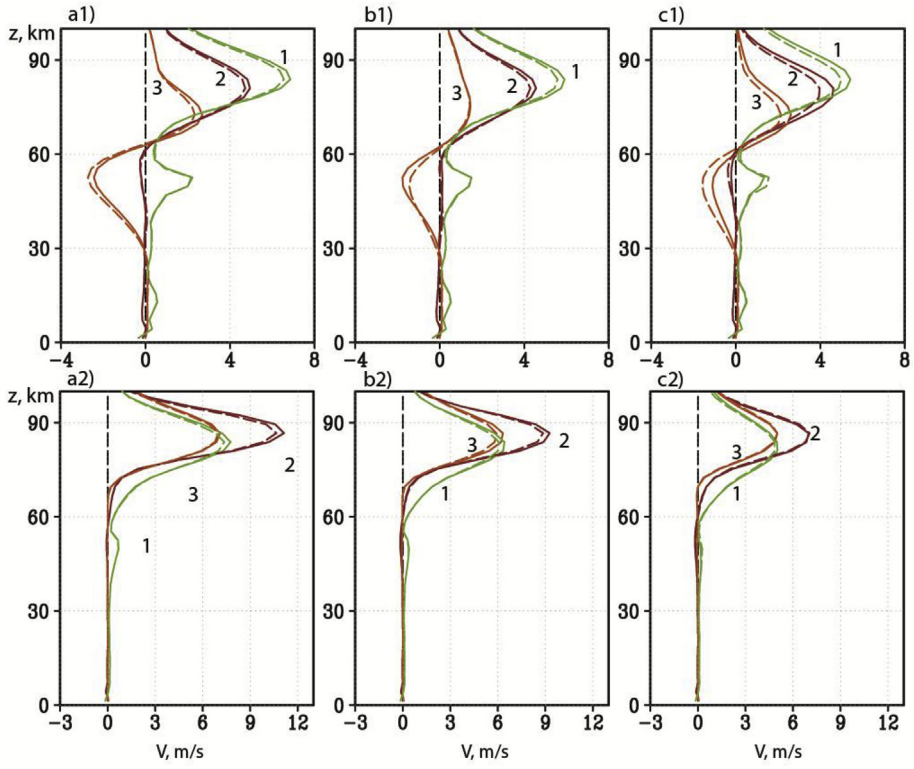

Fig. 4. Meridional velocity in m/s averaged over latitude bands 0 - 30° (1), 30–60° (2) and 60–90° (3) for time intervals before (a), during (b) and after (c) simulated SWs for the Northern (winter) Hemisphere (1st row) and the Southern (summer) Hemisphere (2nd row). Solid and dashed lines correspond to simulations including and excluding OGW effects.

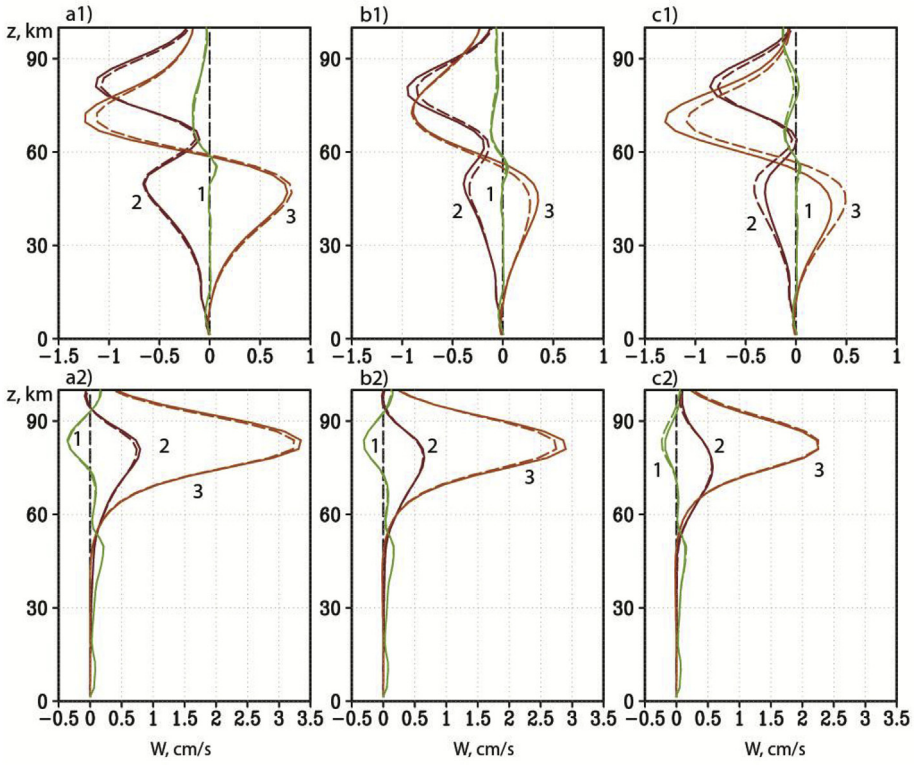

Fig. 5. The same as Fig. 4, but for the vertical velocity in cm/s.

Fig. 2c reveals average differences in the zonal-mean meridional wind between model runs with thermal and dynamical OGW effects included and excluded in the MUAM for January. The differences have the same signs as peak meridional velocities in Fig. 2b. Maximum differences in Fig. 2c occur at middle and high latitudes of the Northern Hemisphere where OGWs have maximum amplitudes (Gavrilov et al., 2013a, 2015). The southward meridional circulation increases at altitudes above 40 km and decreases below 40 km due to OGW impact, which brings the results of simulations closer to JRA-55 reanalysis data shown in Fig. 2a. Therefore, inclusion of OGW parameterization into the MUAM helps to achieve better agreements between simulated and observed mean meridional circulation.

Fig. 6 shows differences in the zonal-mean meridional (left panels) and vertical (right panels) winds between the MUAM runs with and without inclusion of OGW dynamical and heating effects in time intervals before, during and after simulated SW events. Meridional velocity differences in the left panels of Fig. 6 at altitudes above 60 km have frequently the same signs as the meridional wind presented in Fig. 3a1. This corresponds to up to 10–15% stronger meridional winds above 60 km after involving OGW effects into the MUAM. Before and during SWs this effect is more noticeable in the Southern Hemisphere, while after SWs it is stronger in the Northern Hemisphere. At altitudes below 60 km at high latitudes of the Northern Hemisphere, OGW effects lead to an increase in northward winds before and after simulated SWs and to their decrease at altitudes 40–70 km during SWs (see the left panels of Fig. 6).

Similar diverse OGW impacts demonstrate differences of vertical velocity in the right panels of Fig. 6. OGW effects increase vertical velocities (up to 10–15%) at high northern latitudes at altitudes 40–60 km during simulated SWs and decrease in this region before and after SWs.

The differences in Fig. 6 indicate a sensitivity of the meridional circulation to the influence of OGWs at different phases of simulated SWs. One of the reasons for this behavior could be significant changes in planetary waves' amplitudes in the atmosphere during SWs (Gavrilov

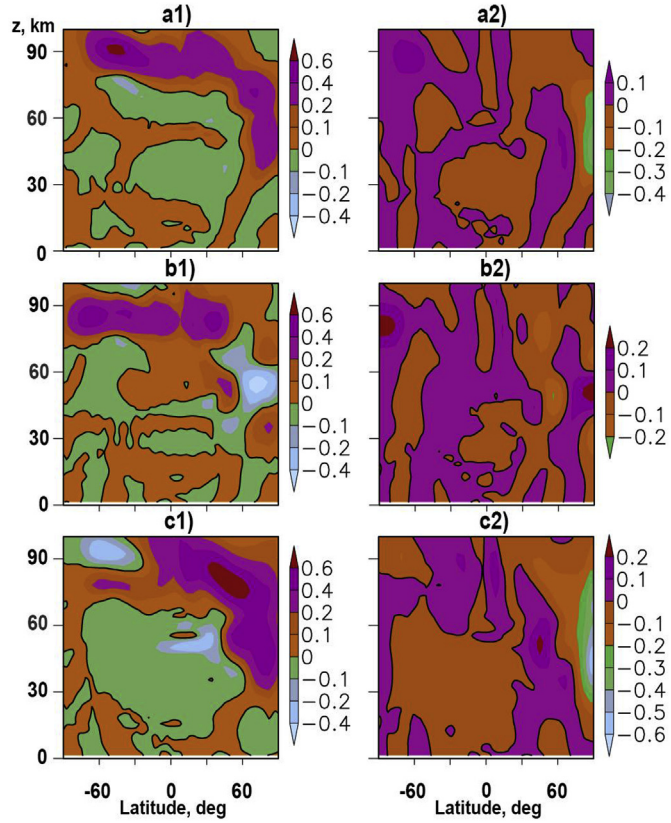

Fig. 6. Average differences in the zonal-mean meridional in m/s (1st column) and vertical in cm/s (2nd column) winds between MUAM runs with and without inclusion of OGW dynamical and heating effects in time intervals before (top), during (middle) and after (bottom) simulated SW events. Solid contours correspond to zero levels.

et al., 2018) due to the OGW effect (Gavrilov et al., 2013a). In addition, the Coriolis force in the equation of motion makes the negative (directed westwards) zonal accelerations created by OGWs, which decelerates the mean eastward atmospheric flow, which corresponds to the negative differences in meridional velocity in Fig. 6b1 at middle latitudes of the Northern Hemisphere.

Figs. 4 and 5 reflect the zonal-mean meridional and vertical velocity components averaged over latitude bands 0–30°, 30–60° and 60–90° (lines marked as 1–3, respectively) of the Northern and Southern Hemispheres before, during and after simulated SW. Solid and dashed lines show velocity components simulated, respectively, including and excluding OGW parameterization to the MUAM. The main integral dynamical effect of stationary OGWs is a drag of zonal atmospheric circulation, which is directed mainly eastwards in the winter Northern Hemisphere. A mechanism of direct OGW influence on meridional circulation could be drag of the mean flow by waves (Andrews et al., 1987). Due to influence of the Coriolis force in the motion equations of the MUAM, negative zonal accelerations of the mean flow produced by OGW correspond to northward add-ons to the meridional wind component. This intensifies meridional circulation at high altitudes in Fig. 4 and increases downward flows in the Northern Hemisphere in the top panels of Fig. 5. Comparisons of solid and dashed lines in Fig. 5a and c shows negative OGW add-ons to the vertical velocity before and after simulated SWs, when zonal flows are eastward and have substantial velocity. These negative add-ons intensify downward flows above altitude of 60 km and decrease upward flows in the latitudinal band 60–90° N at altitudes 15–60 km in Fig. 5a1 and 5c1. Smaller upward motions at northern high-latitudinal stratosphere diminish compensating downward motions at northern mid-latitude stratosphere (lines 2 in Fig. 5a1 and 5c1).

During simulated SWs, eastward winds in the high-latitude stratosphere decrease substantially, therefore OGW drag of the zonal flow produces can produce negative add-ons to meridional wind and positive add-ons to the vertical wind at altitudes 15–60 km in the high-latitude northern band (lines 3 in Fig. 5b1). Intensifying vertical flows there can produce larger compensating downward flows in the northern mid-latitude stratosphere during simulated SWs (lines 2 in Fig. 5b1). Therefore, different signs of add-ons produced by OGW effects in different SW phases may be connected with decreases and reversals of the zonal flow at high latitudes in the winter middle atmosphere during SW events.

Our numerical experiments showed that the meridional mean circulation is sensitive to the dynamical and thermal OGW impacts. Accounting of the OGW influence in the MUAM improve the results and makes the simulated circulation characteristics closer to the observed ones.

4. Conclusions

In this paper, numerical experiments with the MUAM model simulating the general circulation at altitudes 0–135 km are described. In these experiments, we focused on the changes of the mean meridional circulation in the middle atmosphere during 11-day time intervals before, during and after simulated SW events. The MUAM contains a recently developed parameterization of OGW thermal and dynamical effects. In order to obtain sufficient confidence, the results of numerical simulations have been averaged over 12 pairs of the MUAM runs with and without the OGW parameterization.

Results of the analysis show a weakening of the mean meridional circulation (up to 30–40%) in time intervals during and after simulated SWs compared to that before the onset of the events. OGW impacts lead in most cases to 10–15% larger mean meridional wind. Below 50 km, the mean meridional circulation changes (up to 15%) due to OGW impacts during all phases of simulated SWs, especially before and after the events. Considering meridional circulation for January and comparing it with the multi-year reanalysis data allow us to conclude that accounting of the OGW effects in the MUAM brings the simulated meridional circulation characteristics closer to the observed ones. The same improvements but on the zonal mean circulation were discussed in the paper of Gavrilov et al. (2013a).

The performed numerical experiment is important for understanding the contributions of different factors to formation of global dynamical processes in the atmosphere. Our study shows that the mean global meridional circulation in the middle atmosphere substantially varies due to OGW dynamical and thermal effects.

Acknowledgements

Improving and adjusting the MUAM for the present study was supported by the Russian Science Foundation (grant #18-77-00022). Numerical simulations and analysis was supported by the Russian Foundation for Basic Research (grants #16-35-60013 mol_a_dk; #18-05-01050). Data provided by the SPbU resource center “Geomodel” have been used.

Appendix A. Supplementary data

Supplementary data to this article can be found online at https://doi.org/10.1016/j.jastp.2018.12.012.

References

Albers, J.R., Birner, T., 2014. Vortex preconditioning due to planetary and gravity waves prior to sudden stratospheric warmings. J. Atmos. Sci. 71, 4028–4054. https://doi.org/10.1175/JAS-D-14-0026.1.

Andrews, D.G., Holton, J.R., Leovy, C.B., 1987. Middle Atmosphere Dynamics. Academic, New York.

Baldwin, M.P., Gray, L.J., Dunkerton, T.J., 2001. The quasi-biennial oscillation. Rev. Geophys. 39 (2), 179–229.

Baldwin, M.P., Dameris, M., Shepherd, T.G., 2007. How will the stratosphere affect climate change? Science 316, 1576–1577.

Buhler, O., 2009. Waves and Mean Flows. Cambridge University Press, pp. 341.

Butchart, N., Scaife, A.A., Bourqui, M., et al., 2006. Simulations of anthropogenic change in the strength of the Brewer-Dobson circulation. Clim. Dynam. 27, 727–741. https://doi.org/10.1007/s00382-006-0162-4.

Butler, A., Seidel, D., Hardiman, S., et al., 2015. Defining sudden stratospheric warmings. Bull. Am. Meteorol. Soc. https://doi.org/10.1175/BAMS-D-13-00173.1.

Catry, B., Geleyn, J.F., Bouyssel, F., Cedilnik, J., Broo, R., Derková, M., Mladek, R., 2008. A new sub-grid scale lift formulation in a mountain drag parameterisation scheme. Meteorol. Z. 17 (2), 193–208.

Charlton, A.J., Polvani, L.M., 2007. A new look at stratospheric sudden warmings. Part I: climatology and modeling benchmarks. J. Clim. 20, 449–469.

Cohen, N., Gerber, E.P., Buhler, O., 2013. Compensation between resolved and unresolved wave driving in the stratosphere: implications for downward control. J. Atmos. Sci. 70, 3780–3798.

Cohen, N., Gerber, E.P., Buhler, O., 2014. What drives the Brewer-Dobson circulation. J. Atmos. Sci. 71 (10), 3837–3855.

de la Camara, A., Abalos, M., Hitchcock, P., 2018. Changes in stratospheric transport and mixing during sudden stratospheric warmings. J. Geophys. Res.: Atmosphere 123 (7), 3356–3373. https://doi.org/10.1002/2017JD028007.

ETOPO2, 2015. Gridded global 2-minute relief data. National geophysical data center, National Oceanic and atmospheric Administration, U.S. Dept. Of Commerce. http://www.ngdc.noaa.gov/mgg/global/etopo2.html, Accessed date: 15 January 2015.

Fröhlich, K., Pogoreltsev, A., Jacobi, Ch, 2003. Numerical simulation of tides, Rossby and Kelvin waves with the COMMA-LIM model. Adv. Space Res. 32, 863–868.

Fuller-Rowell, T., Wu, F., Akmaev, R., Fang, T.-W., Araujo-Pradere, E., 2010. A whole atmosphere model simulation of the impact of a sudden stratospheric warming on thermosphere dynamics and electrodynamics. J. Geophys. Res. 115, A00G08. https://doi.org/10.1029/2010JA015524.

Funke, B., Lopez-Puertas, M., Bermejo-Pantaleon, D., Garcia-Comas, M., Stiller, G.P., von Clarmann, T., Kiefer, M., Linden, A., 2010. Evidence for dynamical coupling from the lower atmosphere to the thermosphere during a major stratospheric warming. Geophys. Res. Lett. 37, L13803. https://doi.org/10.1029/2010GL043619.

Gavrilov, N.M., Koval, A.V., 2013. Parameterization of mesoscale stationary orographic wave impact for usage in numerical models of atmospheric dynamics. Izvestiya Atmos. Ocean. Phys. 49 (3), 243–251.

Gavrilov, N.M., Pogoreltsev, A.I., Jacobi, Ch, 2005. Numerical modeling of the effect of latitude-inhomogeneous gravity waves on the circulation of the middle atmosphere. Izvestiya Atmos. Ocean. Phys. 41 (1), 9–18.

Gavrilov, N.M., Koval, A.V., Pogoreltsev, A.I., Savenkova, E.N., 2013a. Numerical simulation of the response of general circulation of the middle atmosphere to spatial inhomogeneities of orographic waves Izvestiya. Atmospheric and Oceanic Physics 49 (4), 367–374.

Gavrilov, N.M., Koval, A.V., Pogoreltsev, A.I., Savenkova, E.N., 2013b. Numerical modeling influence of inhomogeneous orographic waves on planetary waves in the

middle atmosphere. Adv. Space Res. 51 (11), 2145–2154.
Gavrilov, N.M., Koval, A.V., Pogoreltsev, A.I., Savenkova, E.N., 2015. Simulating influences of QBO phases and orographic gravity wave forcing on planetary waves in the middle atmosphere. Earth Planets Space 67, 86. https://doi.org/10.1186/s40623-015-0259-2.
Gavrilov, N.M., Koval, A.V., Pogoreltsev, A.I., Savenkova, E.N., 2018. Simulating planetary wave propagation to the upper atmosphere during stratospheric warming events at different mountain wave scenarios. Adv. Space Res. 61 (I. 7), 1819–1836. https://doi.org/10.1016/j.asr.2017.08.022.
Gelaro, R., McCarty, W., Suárez, M.J., Todling, R., Molod, A., Takacs, L., et al., 2017. The modern-era retrospective analysis for Research and applications, version 2 (MERRA-2). J. Clim. 30 (14), 5419–5454. https://doi.org/10.1175/JCLI-D-16-0758.1.
Geller, M.A., Zhou, T., Ruedy, R., 2011. New gravity wave treatments for GISS climate models. J. Clim. 24, 3989–4002. https://doi.org/10.1175/2011JCLI4013.1.
Gossard, E.E., Hooke, W.H., 1975. Waves in the Atmosphere. Elsevier Sci. Publ. Co., Amsterdam-Oxford-New York.
Holton, J.R., Mass, C., 1976. Stratospheric vacillation cycles. J. Atmos. Sci. 33, 2218 2215.
Kim, Y.-J., Arakawa, A., 1995. Improvement of orographic gravity wave parameterization using a mesoscale gravity wave model. J. Atmos. Sci. 52 (11), 1875–1902.
Kobayashi, S., Ota, Y., Harada, H., 2015. The JRA-55 reanalysis: general specifications and basic characteristics. J. Meteorol. Soc. Jpn. 93, 5–48. https://doi.org/10.2151/jmsj.2015-00.
Koval, A.V., Gavrilov, N.M., Pogoreltsev, A.I., Savenkova, E.N., 2018. Comparisons of planetary wave propagation to the upper atmosphere during stratospheric warming events at different QBO phases. J. Atmos. Sol. Terr. Phys. 171, 201–209. https://doi.org/10.1016/j.jastp.2017.04.013.
Kurihara, J., Ogawa, Y., Oyama, S., Nozawa, S., Tsutsumi, M., Hall, C.M., Tomikawa, Y., Fujii, R., 2010. Links between a stratospheric sudden warming and thermal structures and dynamics in the high-latitude mesosphere, lower thermosphere, and ionosphere. Geophys. Res. Lett. 37, L13806. https://doi.org/10.1029/2010GL043643.
Kuttippurath, J., Nikulin, G., 2012. The sudden stratospheric warming of the Arctic winter 2009/2010: comparison to other recent warm winters. Atmos. Chem. Phys. Discuss. 12, 7243–7271.
Labitzke, K., 1977. Interannual variability of the winter stratosphere in the Northern hemisphere. Mon. Weather Rev. 105, 762–770.
Labitzke, K., Kunze, M., 2009. On the remarkable Arctic witer in 2008/2009. J. Geophys. Res. 114, D00102. https://doi.org/10.1029/2009JD012273.
Lindzen, R.S., 1981. Turbulence and stress owing to gravity wave and tidal breakdown. J. Geophys. Res. 86, 9707–9714.
Liu, H., Doornbos, E., Yamamoto, M., Ram, S.T., 2011. Strong thermospheric cooling during the 2009 major stratosphere warming. Geophys. Res. Lett. 38, L12102. https://doi.org/10.1029/2011GL047898.
Longuet-Higgins, M.S., 1968. The eigenfunctions of Laplace's tidal equation over a sphere. Phil. Trans. Roy. Soc. Lond. 262, 511–607.
Lott, F., Miller, M.J., 1997. A new subgrid-scale orographic drag parametrization: its formulation and testing. Q. J. R. Meteorol. Soc. 123, 101–127.
Masakazu, T., 2003. Tropospheric response to stratospheric sudden warmings in a simple global circulation model. J. Clim. 16, 3039–3049.
Matsuno, T., 1966. Numerical integration of the primitive equations by a simulated backward difference method. J. Meteorol. Soc. Jpn. 44, 76–84.
McInturff, R.M., 1978. Stratospheric warmings: synoptic, dynamic, and general circulation aspects. NASA Ref. Publ. 1017, 1–174.
McIntyre, M.E., 1982. How well do we understand the dynamics of stratospheric warmings. J. Meterol. Soc. Japan. 60, 37–64.
McLandress, C., McFarlane, N.A., 1993. Interactions between orographic gravity wave drag and forced stationary planetary waves in the winter Northern Hemisphere middle atmosphere. J. Atmos. Sci. 50 (13), 1966–1990.
Nath, D., Chen, W., Zelin, C., Pogoreltsev, A.I., Wei, K., 2016. Dynamics of 2013 Sudden Stratospheric Warming event and its impact on cold weather over Eurasia: role of planetary wave reflection. Sci. Rep. 6, 24174. https://doi.org/10.1038/srep24174.
Pogoreltsev, A.I., 2007. Generation of normal atmospheric modes by stratospheric vacillations. Izvestiya Atmos. Ocean. Phys. 43 (4), 423–435.
Pogoreltsev, A.I., Vlasov, A.A., Froehlich, K., Jacobi, Ch, 2007. Planetary waves in coupling the lower and upper atmosphere. J. Atmos. Sol. Terr. Phys. 69, 2083–2101. https://doi.org/10.1016/j.jastp.2007.05.014.
Pogoreltsev, A.I., Kanukhina, A. Yu, Suvorova, E.V., Savenkova, E.N., 2009. Variability of planetary waves as a signature of possible climatic changes. J. Atmos. Sol. Terr. Phys. 71, 1529–1539. https://doi.org/10.1016/j.jastp.2009.05.011.
Pogoreltsev, A.I., Savenkova, E.N., Pertsev, N.N., 2014. Sudden stratopheric warmings: the role of normal atmospheric modes. Geomagn. Aeron. 54 (3), 357–372.
Quiroz, R., 1975. Stratospheric evolution of Sudden warmings in 1969-74 determined from measured infrared radiation fields. J. Atmos. Sci. 32, 211–224.
Rice, J.A., 2006. Mathematical Statistics and Data Analysis, third ed. Duxbury Press.
Rienecker, M.M., Suarez, M.J., Gelaro, R., Todling, R., Bacmeister, J., Liu, E., Bosilovich, M.G., Schubert, S.D., Takacs, L., Kim, G.-K., et al., 2011. MERRA: NASA's modern-era retrospective analysis for research and applications. J. Climate 14, 3624–3648. https://doi.org/10.1175/JCLI-D-11-00015.1.
Swinbank, R., O'Neill, A., 1994. Stratosphere-troposphere assimilation system. Mon. Weather Rev. 122, 686–702.
Savenkova, E.N., Gavrilov, N.M., Pogoreltsev, A.I., 2017. On statistical irregularity of stratospheric warming occurrence during northern winters. J. Atmos. Sol. Terr. Phys. 163, 14–22. https://doi.org/10.1016/j.jastp.2017.06.007.
Schoeberl, M., 1978. Stratospheric warmings – observations and theory. Rev. Geophys. 16, 521–538. https://doi.org/10.1029/RG016i004p00521.
Scinocca, J.F., McFarlane, N.A., 2000. The parameterization of drag induced by stratified flow over anisotropic orography. Q. J. R. Meteorol. Soc. 126 (568), 2353–2393.
Sigmond, M., Shepherd, T.G., 2014. Compensation between resolved wave driving and parameterized orographic gravity wave driving of the Brewer–Dobson circulation and its response to climate change. J. Clim. 27 (14), 5601–5610.
Siskind, D.E., Eckermann, S.D., McCormack, J.P., Coy, L., Hoppel, K.W., Baker, N.L., 2010. Case studies of the mesospheric response to recent minor, major and extended stratospheric warmings. J. Geophys. Res. 115, D00N03. https://doi.org/10.1029/2010JD014114.
Sun, L., Robinson, W.A., 2009. Downward influence of stratospheric final warming events in an idealized model. Geophys. Res. Lett. 36, L03819. https://doi.org/10.1029/2008GL036624.
Swarztrauber, P.N., Kasahara, A., 1985. The vector harmonic analysis of Laplace's tidal equations. SIAM J. Sci. Stat. Comput. 6, 464–491.
Tao, M.C., Liu, Y., Zhang, Y.L., 2017. Variation in Brewer–Dobson circulation during three sudden stratospheric major warming events in the 2000s. Adv. Atmos. Sci. 34 (12), 1415–1425. https://doi.org/10.1007/s00376-017-6321-1.
Vosper, S.B., Brown, A.R., 2007. The effect of small-scale hills on orographic drag. Q. J. R. Meteorol. Soc. 133, 1345–1352.
Yuan, T., Thurairajah, B., She, C.-Y., Chandran, A., Collins, R.L., Krueger, D.A., 2012. Wind and temperature response of midlatitude mesopause region to the 2009 sudden stratospheric warming. J. Geophys. Res. 117, D09114. https://doi.org/10.1029/2011JD017142.